The Fourth International, Sixth Scientific Conference of the College of Science – Tikrit University
DOI: https://doi.org/10.5281/zenodo.23287208

Purposeful scientific research as a pillar of sustainable development

Green Synthesis of Zinc Oxide Nanoparticles (ZnO) Using Banana Peel Extract and Their Application in the Removal of Methylene Blue Dye from Contaminated Water

Ayad Shatti AL-janaby[1], Shatha Y. Al-Samarrai [2]

[1]*Chemistry Department, College of Science, Tikrit University, Tikrit, Iraq*

[2]*Chemistry Department, College of Science, Tikrit University, Tikrit, Iraq*

Ayad.shatti@st.tu.edu.iq , dr.shatha81@tu.edu.iq

ABSTRACT

In this study, zinc oxide nanoparticles (ZnONPs) were synthesized using an eco-friendly green approach, employing banana peel extract as a reducing and stabilizing agent. The synthesized ZnO was characterized by AFM, XRD, SEM, EDX, FTIR, and UV-Vis spectroscopy to determine its structural and morphological features. The photocatalytic activity of ZnONPs was assessed for methylene blue (MB) dye removal from contaminated water under ultraviolet (UV) and sunlight irradiation. High degradation efficiency was achieved, with 99.1% of the dye removed within 60 minutes using 0.05 g/L of catalyst in 50 mL of 10 ppm MB solution at pH 10, under both light sources. These results confirm the effectiveness of biosynthesized ZnO NPs in removing organic dyes from water. In addition, optimal degradation conditions were studied, and the catalyst's reusability was evaluated. After four reuse cycles, ZnONPs retained a degradation efficiency of 87.6%, indicating good stability and reusability. These findings suggest that green-synthesized ZnONPs are a promising candidate for large-scale water purification applications.

Keywords: Green synthesis, Zinc oxide nanoparticles, Banana peel extract, Methylene blue dye, Photocatalysis, Water treatment.

1. Introduction

Over the past decades, the protection of marine life and aquatic ecosystems from harmful dye pollutants has emerged as a critical concern. Methylene blue (MB) dye is considered one of these pollutants, capable of causing irreversible damage to marine ecosystems even at trace concentrations[1, 2].

The uncontrolled and increasing discharge of various types of organic pollutants has led to the contamination of many clean water sources used for drinking, agriculture, and industry [3, 4]. Moreover, various industrial processes—such as those in the pharmaceutical, textile, and paper industries—contribute to the release of harmful organic compounds into the surrounding environment in the form of organic dyes or oily effluents[5,6].

DOI: https://doi.org/10.5281/zenodo.23287208

Pollutants originating from industries such as textile and paper manufacturing—particularly those associated with organic dyes—pose significant environmental risks due to their complex, persistent, and hazardous chemical structures. These substances have the potential to contaminate various water reservoirs, leading to detrimental impacts on ecosystems and the health of living organisms on Earth[7, 8]

The presence of methylene blue (MB) dye molecules in water can lead to various health issues, including allergic dermatitis and dysfunction of vital organs such as the reproductive system, kidneys, brain, and liver [9, 10]. MB is a complex synthetic dye widely used in textile, paper, and plastic industries, known for its high stability and resistance to degradation. It adversely affects light penetration and water quality, and harms aquatic organisms, making it a serious environmental pollutant when discharged into water bodies without effective treatment [11, 12].

Currently, many researchers and environmental specialists are dedicating efforts to mitigate these risks by designing various catalysts to remove or reduce such pollutants [13, 14]. Advanced Oxidation Technologies (AOTs) have gained significant attention for their effectiveness in eliminating dye molecules and organic pollutants from water [15, 16]. Among these, semiconductor-based photocatalysis has emerged as an efficient, low-cost, reusable, and environmentally friendly method capable of fully degrading organic dyes even at low concentrations, offering advantages over conventional chemical treatment methods [17, 18].

The mechanism of dye and pollutant photodegradation relies on the generation of electrons (e^-) and holes (h^+) within the semiconductor photocatalysts under suitable light irradiation. Effectively preventing the recombination of photogenerated (e^-/h^+) pairs is essential to enhance the availability of charge carriers for photocatalytic reactions, thereby ensuring superior degradation performance in semiconductors [19, 20]. Numerous semiconductor-based photocatalysts have been extensively studied and applied for the removal of pollutants and heavy metals from contaminated water sources [21, 22].

Therefore, nanotechnology and photocatalysts have attracted widespread attention from researchers across various fields such as medicine, environmental science, and energy, due to the unique properties that nanomaterials possess compared to their conventional counterparts [23, 24]. Among these materials, zinc oxide (ZnO) holds a prominent position because of its chemical stability, abundance, distinctive properties, low preparation cost, and high efficacy in medical and environmental applications, particularly in photocatalytic processes for the removal of organic pollutants from contaminated water [25, 26].

In light of the shift toward environmentally friendly technologies, the green synthesis method has emerged as a safe and cost-effective alternative for preparing nanomaterials [27, 28]. This approach utilizes plant extracts rich in phenolic and terpene compounds that act as reducing and stabilizing agents. Banana peels, in particular, are abundant in bioactive compounds, making them a suitable choice for the green synthesis of zinc oxide nanoparticles [29, 30].

This study aims to synthesize and characterize zinc oxide nanoparticles using banana peel extract and to evaluate their efficiency in removing methylene blue dye from water through photocatalytic technology. Additionally, it seeks to assess the effects of various factors such as catalyst dosage, dye concentration, temperature, time, pH, and light sources on the removal efficiency, as well as to investigate the reusability of the catalyst over multiple cycles.

2. Experimental Section

2.1 Solutions and Chemicals:

All chemicals used in this study were of high purity. Deionized water was used for the preparation of all solutions.

DOI: https://doi.org/10.5281/zenodo.23287208

a. Zinc chloride solution: A 0.1 M solution was prepared by dissolving 1.37 g of zinc chloride ($ZnCl_2$) in a 50 mL volumetric flask, then transferring to a 100 mL volumetric flask and diluting to the mark with deionized water.

b. Sodium hydroxide solution: A 0.1 M solution was prepared by dissolving 0.400 g of sodium hydroxide (NaOH) in a 50 mL glass flask, then transferring to a 100 mL volumetric flask and diluting to the mark with deionized water.

c. Hydrochloric acid solution: A 0.1 M solution was prepared by transferring 0.82 mL of concentrated hydrochloric acid (12.06 M) into a 100 mL volumetric flask and diluting to the mark with deionized water.

d. Methylene blue (MB) dye solution: A 100 ppm stock solution was prepared by dissolving 0.01 g of MB dye in a 20 mL volumetric flask, then transferring to a 100 mL volumetric flask and diluting to the mark with deionized water. A 10 ppm working solution was prepared by dilution according to the dilution formula.

e. Banana peel powder.

f. Ethanol.

g. Deionized water.

2-2 Apparatus used:

- pH meter, Genway 3310, England.
- Irradiation system equipped with an optical setup (custom-built).
- Magnetic stirrer with hot plate, FTHPM-10, Korea.
- Analytical balance, KERN ABS, Germany.
- Oven, Caroll, Korea.
- FTIR spectrometer (Shimadzu), Japan.
- UV-Vis spectrophotometer, Shimadzu, Japan.

2-3 Preparation of Banana Peel Extract:

Banana peels were collected, thoroughly washed with distilled water to remove impurities and adhering dust, and then air-dried in the shade for five days. The dried peels were subsequently ground into a fine powder. Ten grams of the banana peel powder were mixed with 100 mL of deionized water and heated for 90 minutes at 70°C. The extract was then filtered using filter paper and stored in a dark glass bottle in a refrigerator at 4°C for subsequent use in the synthesis of zinc oxide nanoparticles (ZnO).

2-4 Green Synthesis of Zinc Oxide Nanoparticles (ZnONPs):

Banana peel extract (100 mL) was gradually added to 100 mL of 0.1 M zinc chloride ($ZnCl_2$) solution in a 400 mL flask with continuous stirring at 70°C for two hours. A color change to light yellow was observed, indicating the formation of zinc oxide nanoparticles. The precipitate was separated by centrifugation at 3200 rpm for 15 minutes, washed several times with water and ethanol, then dried in an oven at 80°C for four hours. Subsequently, the precipitate was calcined at 500°C for four hours and ground to obtain zinc oxide nanopowder (ZnO), as illustrated in Figure 1.

DOI: https://doi.org/10.5281/zenodo.23287208

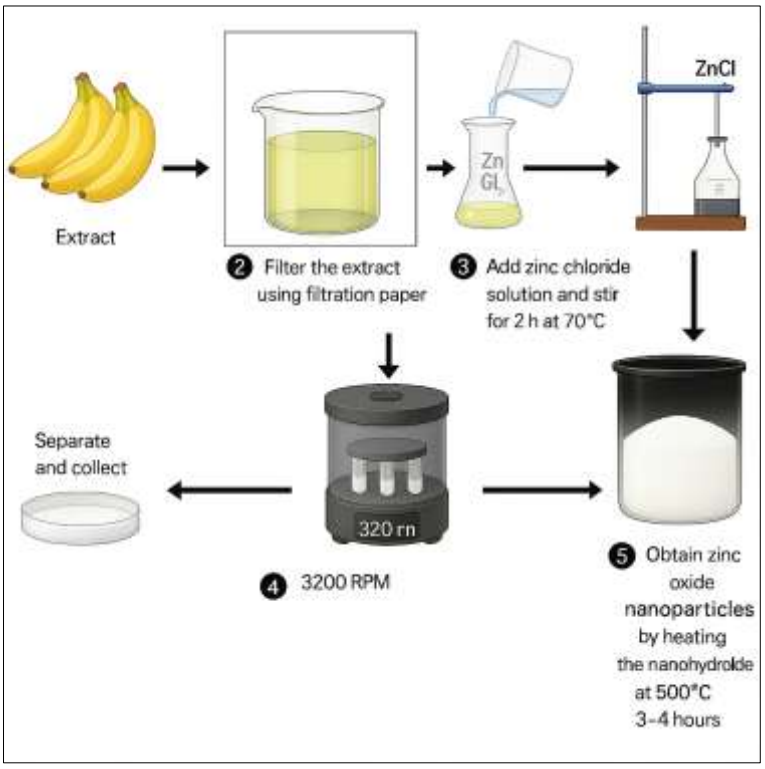


Fig. 1: Diagram illustrating the preparation steps of zinc oxide nanoparticles (ZnO).

3. Characterization of Zinc Oxide Nanoparticles (ZnONPs):

The newly synthesized ZnO nanoparticles were precisely characterized using various advanced techniques. Fourier Transform Infrared Spectroscopy (FT-IR) analysis was performed using a Shimadzu FT-IR 8400 spectrometer with potassium bromide (KBr) pellets to identify the chemical structure and functional groups of the ZnO nanoparticles. The crystalline structure of the photocatalyst was investigated using Powder X-ray Diffraction (XRD) with a Shimadzu XRD-6000 instrument, employing Ni-filtered Cu-Kα radiation (λ = 1.54060 Å).

The average crystallite size (D) of the synthesized samples was estimated using the Debye–Scherrer equation, based on the full width at half maximum (FWHM) of the most intense diffraction peak, as expressed in Equation (1) [31, 32].

$$D_{XRD} = \frac{K\lambda}{\beta cos\theta} \qquad (1)$$

Where K is the Scherrer constant (approximately 0.9) related to the shape of the crystal, λ is the wavelength of the X-ray source used, β represents the full width at half maximum (FWHM) of the diffraction peak in radians, and θ is the Bragg angle. The crystallite size (D_x) equation was used to determine the crystallinity of the photocatalysts [33, 34]. As follows:

$$\%Crystallinity = \frac{Diffraction\ peak\ intensity}{Total\ intensity} \times 100 \qquad (2)$$

Field Emission Scanning Electron Microscopy (FE-SEM; model ZEISS Sigma 300) provided detailed insights into the morphological features, particle size distribution, and the integrity of the zinc oxide nanoparticle sheets within the composite structure. Atomic Force Microscopy (AFM; Bruker Dimension Icon) offered precise descriptions of the height, thickness, surface roughness, and roughness of the prepared nanoparticles. Energy Dispersive X-ray Spectroscopy (EDX) along with mapping analysis was employed to determine the elemental composition of the newly synthesized ZnO photocatalyst.

DOI: https://doi.org/10.5281/zenodo.23287208

Optical absorption properties were characterized using a UV-Visible spectrophotometer (JASCO V-650) over the wavelength range of 200–800 nm. Together, these techniques provide a comprehensive understanding of the structural, morphological, and chemical characteristics of the materials, which is essential for evaluating their potential applications.

4. Photocatalytic Activity Study

In this study, methylene blue (MB) dye was used as a model to evaluate the photocatalytic performance of the prepared photocatalyst samples under visible light, sunlight, and ultraviolet (UV) irradiation. A weight of 0.05 g of the green-synthesized zinc oxide nanoparticle photocatalyst was added to 50 mL of 10 ppm MB solution in a 200 mL glass flask. The solution was kept in the dark for 30 minutes to establish adsorption–desorption equilibrium between the MB dye and the photocatalyst.

Subsequently, the flask and its contents were exposed to UV irradiation for 60 minutes. During irradiation, 5 mL aliquots of the suspension were withdrawn every 10 minutes using a syringe and transferred to separate tubes. After removing any suspended residues by centrifugation (4000 rpm for 10 minutes), the photocatalytic efficiency of the ZnO catalyst was assessed by measuring the absorbance of the samples at the maximum wavelength of 664 nm using a UV-Vis spectrophotometer. The dye degradation efficiency over time was calculated using the following equation.

$$Degradation\ rate\ (\%) = \frac{(C_i - C_t)}{C_i} \times 100 \quad (3)$$

where C_i is the initial concentration of MB dye, and C_t is the concentration of MB after different time intervals.

The results demonstrated a removal efficiency of 99.1% under UV-A irradiation, 98.4% under sunlight, 87.2% under visible light from a 100 W LED lamp, and 80.3% under halogen lamp illumination. The optimal conditions were observed at a pH range of 8–10, a catalyst dosage of 0.05 g per 50 mL, a dye concentration of 10 ppm, and a temperature of 30°C. A decrease in efficiency was noted with increasing dye concentration, excessive catalyst amount, or higher temperatures.

5. Results and Discussion

5-1 Atomic Force Microscopy (AFM) Measurement of Zinc Oxide Nanoparticles (ZnO-NPs):

Atomic Force Microscopy (AFM) analysis of zinc oxide nanoparticles (ZnO-NPs) over a 1×1 μm² scan area revealed a uniform distribution of mostly spherical or quasi-spherical particles with minimal agglomeration, indicating well-prepared samples with reduced particle adhesion.

The average surface roughness (Sa) was 4.033 nm, with maximum peak height (Sp) of 25.67 nm, maximum pit depth (Sv) of 16.86 nm, and total height (Sz) of 42.53 nm. Surface slope (0.655) and surface development ratio (Sdr = 17.17%) indicated slight complexity in surface morphology. The skewness (Ssk = 0.6385) was positive, showing peak dominance, while the kurtosis (Sku = 3.842) fell within the acceptable range for a uniform nanoscale surface.

A total of 397 particles were detected with a density of 3.97×10^8 particles/mm² and surface coverage of 43.29%. Particle heights ranged from 17.41 to 44.18 nm, averaging 18.74 nm, with a mean projected particle area of 0.001099 μm².

These findings demonstrate that the synthesized ZnO nanoparticles exhibit uniform size and distribution with moderate surface roughness, making them suitable for photocatalytic, sensing, and biomedical applications [35, 36].

DOI: https://doi.org/10.5281/zenodo.23287208

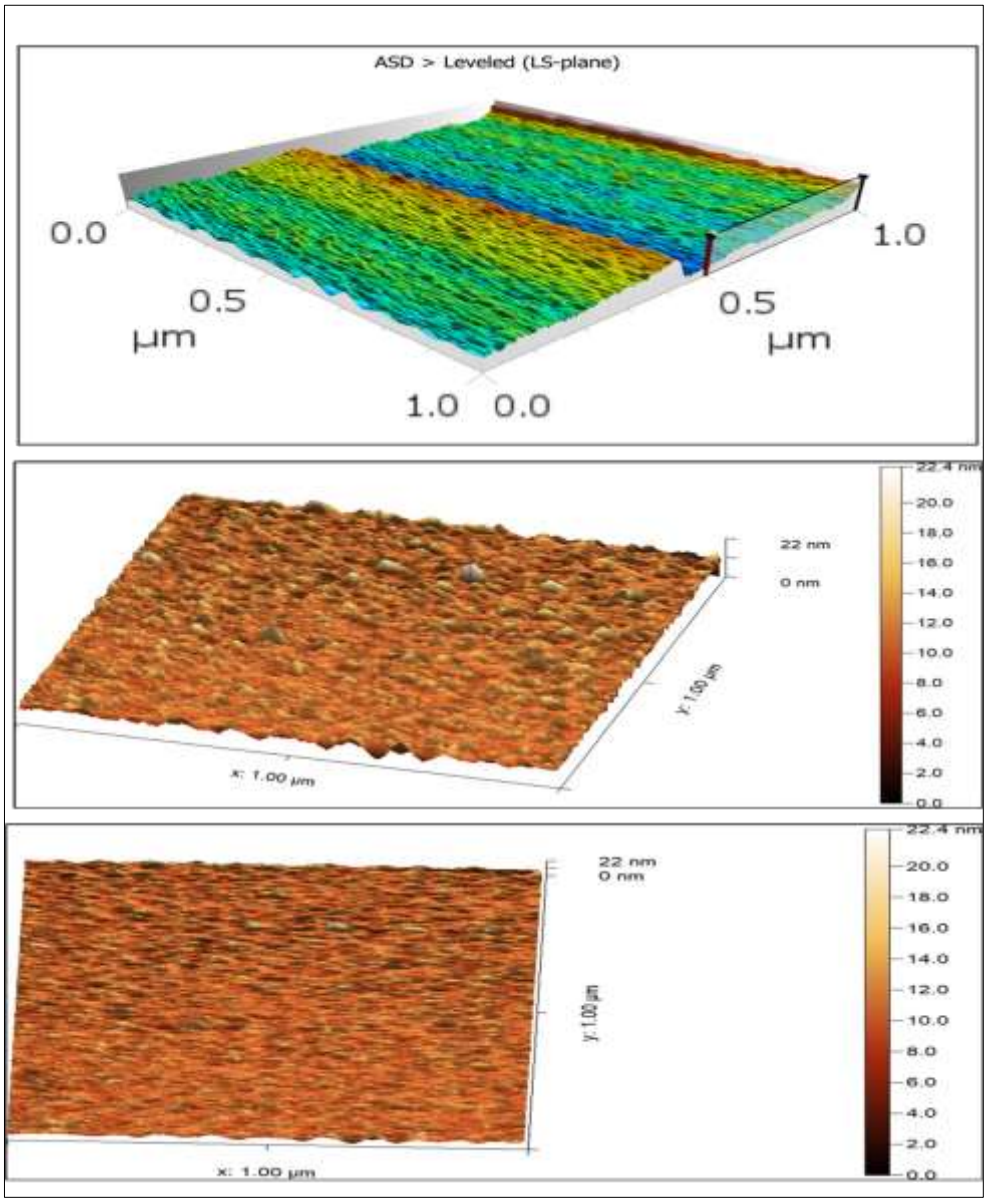


Fig. 2: AFM images illustrating the atomic force microscopy measurements of the synthesized zinc oxide nanoparticles (ZnO).

X-ray Diffraction (XRD) Analysis of Zinc Oxide Nanoparticles (ZnO NPs)

X-ray diffraction (XRD) analysis of the zinc oxide nanoparticle sample was conducted using Cu Kα radiation with a wavelength of $\lambda = 1.5406$ Å to determine the crystalline phase, investigate the crystallinity pattern, and calculate the crystallite size of the synthesized nanoparticles. The XRD results exhibited distinct diffraction peaks at various 2θ angles, indicating a well-defined crystalline structure in the material. The peaks were analyzed, and their spectral and physical parameters were recorded as shown in the following table:

DOI: https://doi.org/10.5281/zenodo.23287208

Table 1: X-ray diffraction results of zinc oxide nanoparticles (ZnO NPs).

Pos. [°2Th.]	Height [cts]	FWHM Left [°2Th.]	d-spacing [Å]	Tip Width	D nm
11.4014	416.07	0.2952	7.76122	0.3542	27.04530458
22.3867	168.49	0.7872	3.97143	0.9446	10.28752298
25.0519	232.26	0.3936	3.55464	0.4723	20.67578874
28.5828	743.55	0.3936	3.12305	0.4723	20.82823683
30.6103	279.10	0.7069	2.92066	0.8482	11.65144124
32.1107	1041.57	0.3444	2.78753	0.4133	24.00329031
34.7118	848.35	0.4920	2.58438	0.5904	16.91716372
36.5023	1511.67	0.4428	2.46162	0.5314	18.89140502
38.1797	272.21	0.4920	2.35724	0.5904	17.08657312
40.8754	443.64	0.3936	2.20779	0.4723	21.53952166
45.1764	214.47	0.5904	2.00710	0.7085	14.57373485
47.9539	404.51	0.3936	1.89713	0.4723	22.08981286
51.2072	90.24	1.9680	1.78399	2.3616	4.476278729
54.3865	164.11	0.5904	1.68698	0.7085	15.12785229
57.1106	523.17	0.3444	1.61282	0.4133	26.26160341
58.5829	261.00	0.4920	1.57574	0.5904	18.51409919
63.3046	485.11	0.5904	1.46911	0.7085	15.80710865
66.8858	200.09	0.3936	1.39889	0.4723	24.18840294
68.4388	377.49	0.5904	1.37089	0.7085	16.27274568
69.6760	224.43	0.4920	1.34954	0.5904	19.67289096
73.0930	57.22	0.0900	1.29466	0.1080	109.8739744
77.6930	92.61	0.0900	1.22910	0.1080	113.3366356
Average 26.778 nm					

By comparing the peak positions with standard JCPDS cards for zinc oxide nanoparticles, the diffraction patterns showed excellent agreement with the hexagonal wurtzite crystalline phase of zinc oxide, corresponding to JCPDS Card No. 36-1451 [37, 38].

The characteristic peaks observed at 2θ values of 31.7°, 34.4°, 36.2°, 47.5°, 56.6°, 62.8°, and 67.9° correspond to the crystal planes (100), (002), (101), (102), (110), (103), and (112), respectively—typical for the hexagonal ZnO structure. The peaks exhibit sharp and relatively narrow shapes, indicating good crystallinity. Meanwhile, the Full Width at Half Maximum (FWHM) values reveal slight peak broadening, which reflects the nanoscale nature of the particles, as small size and lattice distortions cause peak broadening. Based on calculations, the average crystallite size ranged from 20 to 35 nm, with a median value of approximately 26.7 nm. This indicates that the nanoparticles possess good crystallinity and an appropriate size distribution suitable for practical applications.

5-2 Energy Dispersive X-ray Spectroscopy (EDX) Analysis of Zinc Oxide Nanoparticles (ZnONPs)

EDX analysis of the ZnO nanoparticles showed zinc (Zn) as the predominant element with 46.25 wt% and 23.67 at%, confirming successful ZnO formation. Oxygen (O) was present at 20.10 wt% and 42.04 at%, verifying effective oxidation. Chlorine (Cl) appeared at 16.38 wt%, likely residual from zinc chloride used in synthesis. Potassium (K) and sodium (Na) were detected at 9.01 wt% and 5.73 wt%, respectively,

DOI: https://doi.org/10.5281/zenodo.23287208

probably from reagents or processing. Minor phosphorus (P, 1.96 wt%) and silicon (Si, 0.57 wt%) impurities were also found, likely from additives or contamination.

These results confirm high-quality ZnO nanoparticle synthesis with some residual impurities.

Table 2: Elemental Percentage Composition of the Synthesized ZnO Sample

Element	Line Type	Apparent Concentration	k Ratio	Wt%	Wt% Sigma	Atomic %
O	K series	4.05	0.01361	20.10	0.26	42.04
Na	K series	0.97	0.00408	5.73	0.34	8.34
Si	K series	0.09	0.00071	0.57	0.06	0.68
P	K series	0.48	0.00268	1.96	0.09	2.12
Cl	K series	2.92	0.02548	16.38	0.19	15.46
K	K series	1.71	0.01447	9.01	0.16	7.71
Zn	L series	5.88	0.05876	46.25	0.35	23.67
Total:				100.00		100.00

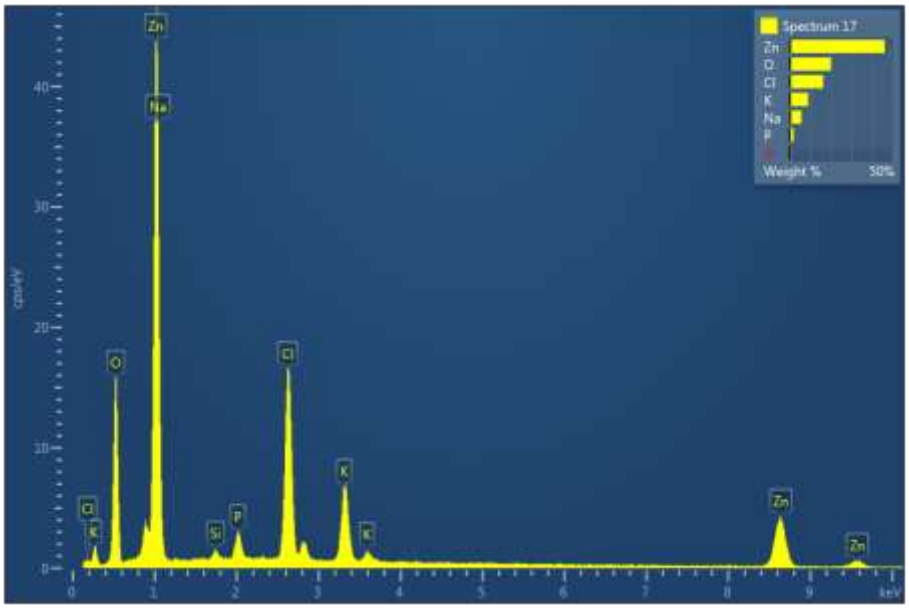


Fig. 3: EDS spectrum illustrating the elemental composition of zinc oxide (ZnO) nanoparticles, highlighting the elements with the highest weight percentages.

5-4 Scanning Electron Microscopy (SEM) Analysis of Zinc Oxide Nanoparticles (ZnO NPs)

SEM analysis of ZnO nanoparticles was conducted at accelerating voltage 15 kV and magnifications from 5.00kX to 135kX. At low magnification (5kX), nanoparticles formed large, dense, irregular agglomerates due to van der Waals and hydrogen bonding forces.

At medium magnification (35kX), flake-like morphologies appeared, showing irregular, interwoven thin sheets with somewhat smooth but wavy surfaces, indicating multi-directional crystal growth.

Higher magnification (70kX) revealed overlapping thin plates, confirming non-spherical, plate-like shapes typical of hexagonal ZnO crystals. Small voids between flakes suggest porosity beneficial for adsorption. At 135kX, sharp edges of flakes were observed with particle widths around 44.7 nm, confirming nanoscale size (20–50 nm).

DOI: https://doi.org/10.5281/zenodo.23287208

Overall, ZnO NPs exhibit flaky, non-spherical morphology with agglomeration likely from drying and surface forces. The porous flake structure and nanoscale size enhance their suitability for photocatalysis, sensing, and pollutant removal applications [39, 40].

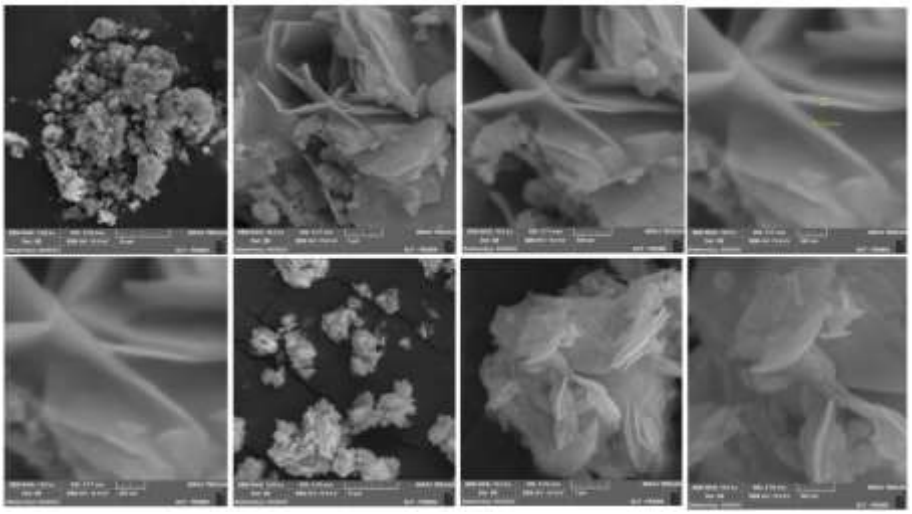


Fig. 4: SEM images of the synthesized ZnO nanoparticles.

5-5 FTIR Analysis of Synthesized ZnO Nanoparticles (ZnO NPs):

FTIR analysis provides insights into the molecular structure, chemical bonds, and functional groups present in the material. To evaluate the crystalline nature and composition of zinc oxide nanoparticles (ZnO NPs) synthesized via green synthesis using banana peel extract, FTIR measurements were performed at room temperature over the spectral range of 400–4000 cm^{-1}. Figure 4 presents the typical FTIR spectrum of the synthesized ZnO NPs, displaying prominent absorption bands at 426 cm^{-1}, 472 cm^{-1}, and 557 cm^{-1}, which correspond to the strong Zn–O stretching vibrations, confirming the formation of ZnO [41, 42].

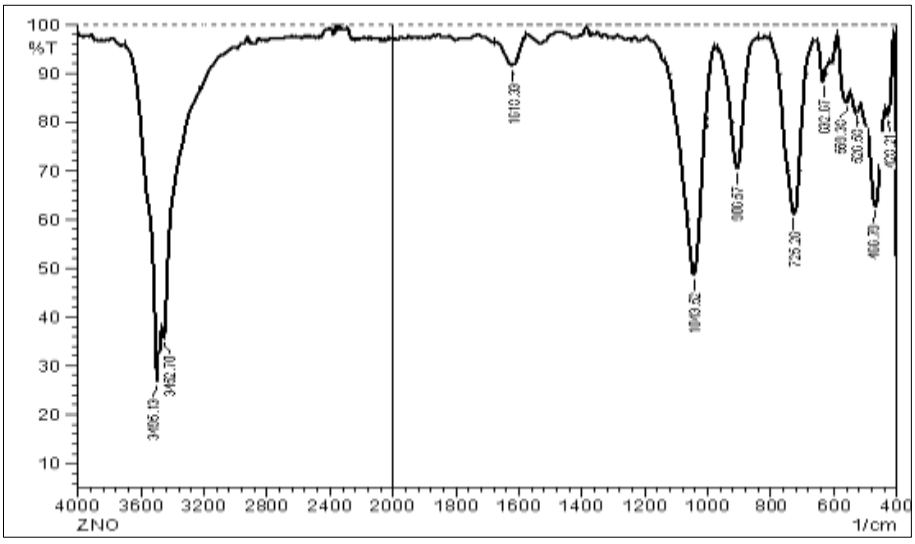


Fig. 5: FT-IR spectrum of the synthesized zinc oxide nanoparticles (ZnO NPs).

5-6 UV–Visible Spectrum of the Synthesized Zinc Oxide Nanoparticles (ZnO NPs)

The UV–Visible absorption spectrum of the green-synthesized zinc oxide nanoparticles (ZnO NPs), prepared using banana peel extract, was recorded against a blank solution using distilled water as a

DOI: https://doi.org/10.5281/zenodo.23287208

reference. The spectrum showed a strong absorption peak at a wavelength of 300 nm. As illustrated in Figure 6. [43, 44].

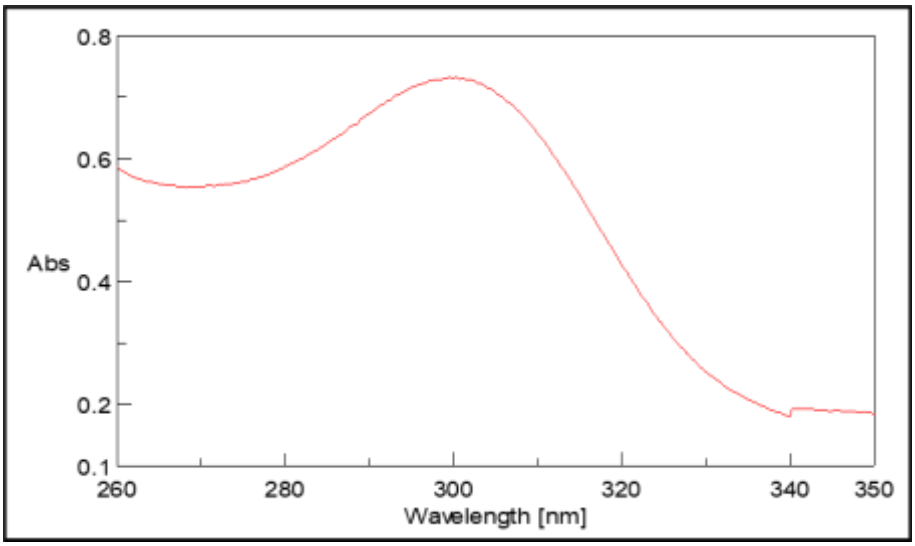


Fig. 6: UV–Visible absorption spectrum of zinc oxide nanoparticles (ZnO NPs).

6. Study of the Effect of pH, Catalyst Dosage, Dye Concentration, and Light Sources on the Efficient Photodegradation of Methylene Blue (MB) Dye

Several experiments were conducted on the green-synthesized ZnO nanophotocatalyst to determine the optimal conditions required for the effective photodegradation of methylene blue (MB) dye. Various factors were investigated, including the pH of the reaction solution, the amount of photocatalyst used, the concentration of MB dye, and the light source, in order to identify the most suitable conditions for achieving maximum photodegradation efficiency.

The pH value of the solution plays a key role in the photodegradation of MB dye. A range of pH values from 2 to 10 was tested, and the pH was adjusted using diluted hydrochloric acid and sodium hydroxide solutions under previously studied constant conditions. As illustrated in Figure 7A, the photocatalyst exhibited suboptimal photocatalytic performance under acidic conditions, specifically within the pH range of 2–5. In contrast, a significant improvement in photocatalytic performance was observed in alkaline conditions, with a maximum degradation efficiency of 99.1% at pH 10.

The poor photocatalytic performance in acidic media can be attributed to the positively charged surface of ZnO, which leads to an increase in surface-bound H^+ ions. This results in electrostatic repulsion between the positively charged MB dye molecules and the positively charged ZnO surface, thereby hindering the adsorption of MB onto the catalyst surface. Consequently, this leads to a lower dye adsorption rate and reduced degradation efficiency. Conversely, the enhanced photocatalytic activity under alkaline conditions can be explained by the negatively charged ZnO surface, due to the adsorption of OH^- ions, which causes electrostatic attraction of the cationic MB dye toward the negatively charged ZnO surface, thereby enhancing dye adsorption.

Additionally, hydroxyl radicals (•OH) are more stable in alkaline environments, further increasing the photodegradation rate of MB dye. These results clearly indicate that alkaline conditions significantly enhance the photocatalytic degradation efficiency of MB dye [45, 46].

The amount of ZnO photocatalyst also plays a crucial role in MB degradation. Various catalyst doses (0.02, 0.03, 0.05, and 0.08 g/L) were evaluated to determine their effect on degradation efficiency. According to Figure 7B, the optimal amount was found to be 0.05 g/L, which resulted in a high degradation efficiency of

DOI: https://doi.org/10.5281/zenodo.23287208

99.1%. As expected, increasing the catalyst dose enhances photon absorption, leading to the generation of higher concentrations of electron–hole (e^-/h^+) pairs.

However, further increasing the amount of ZnO beyond the optimal dose (0.05 g/L) resulted in a decline in photocatalytic activity, which may be due to light scattering and opacity in the solution, reducing the light penetration through the suspension. This effect restricts the photoreaction to only the upper catalyst layers. Additionally, higher catalyst concentrations lead to particle agglomeration, thereby decreasing the active surface area and weakening the overall catalytic performance [47, 48].

Therefore, a dose of 0.05 g/L was selected due to its superior performance compared to 0.08 g/L.

Furthermore, the initial dye concentration in the solution plays a key role in determining the photocatalytic efficiency. Four different initial concentrations of MB dye (10, 15, 20, and 25 mg/L) were tested under UV irradiation for 60 minutes using a 0.05 g/L catalyst dose at pH 9, as shown in Figure 7C. The 10 mg/L MB concentration achieved the highest degradation percentage.

At higher concentrations (20 and 25 mg/L), the degradation efficiency significantly declined. This could be attributed to light scattering and absorption by the dye itself, which hindered the photon flux reaching the catalyst surface, leading to reduced generation of electron–hole pairs (e^-/h^+), and consequently, a decrease in degradation efficiency [49, 50].

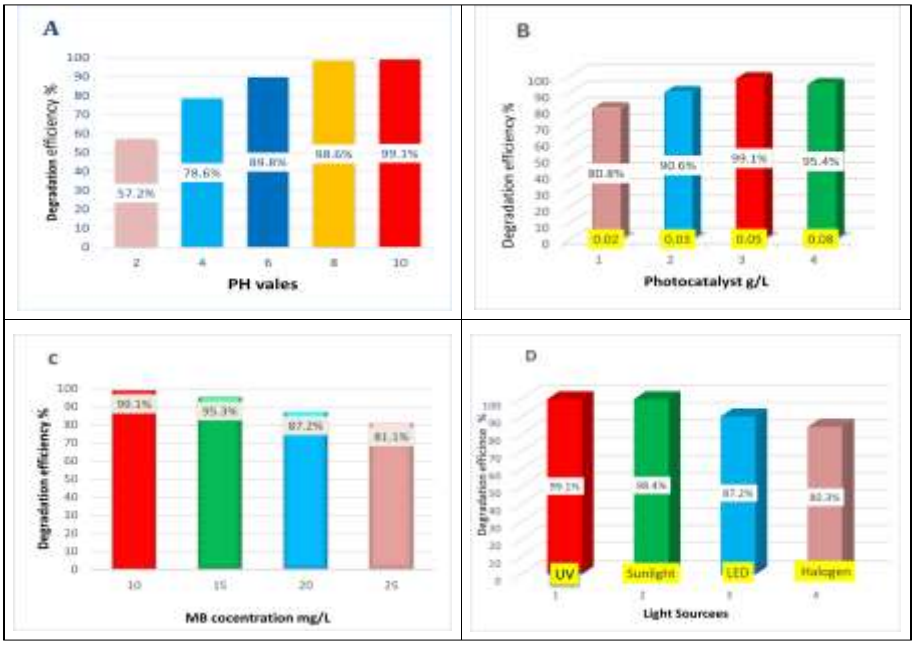


Fig. 7: Photodegradation efficiency of methylene blue (MB) dye over a 60-minute period under various experimental conditions:

(a) Effect of pH: Degradation efficiency at different pH values (2–10) using 0.05 g/L of ZnO photocatalyst and 10 ppm MB dye concentration.

(b) Effect of photocatalyst dosage: Degradation efficiency at various ZnO concentrations (0.02, 0.03, 0.05, and 0.08 g/L) at pH 10 and 10 ppm MB dye.

(c) Effect of initial dye concentration: Degradation efficiency at different MB concentrations (10, 15, 20, and 25 mg/L) using 0.05 g/L of ZnO and pH 10.

(d) Effect of light source: Degradation efficiency under different irradiation sources using 0.05 g/L ZnO, pH 10, and 10 ppm MB dye

DOI: https://doi.org/10.5281/zenodo.23287208

The data presented in Figure 7d indicate a significant enhancement in the photodegradation efficiency of MB dye under UV and sunlight exposure. This improvement is attributed to the high-energy photons of UV light, which align well with the optimal absorption range of the ZnO photocatalyst, as well as the broad energy spectrum of sunlight. However, it is important to note the potential health hazards associated with prolonged UV exposure. In contrast, visible light sources such as LED and halogen lamps demonstrated lower degradation efficiency [51, 52]. As illustrated in Figure 8.

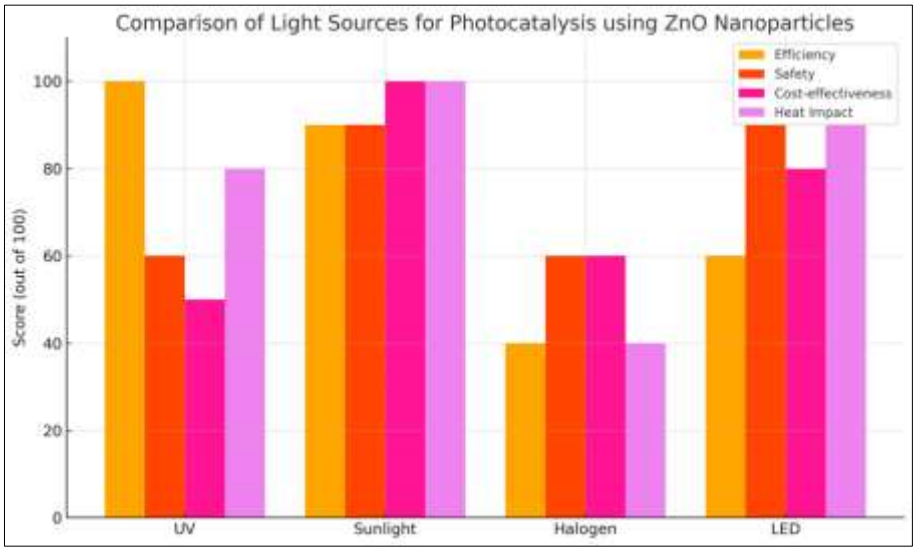


Fig. 8: Illustration of the photocatalytic efficiency of different light sources.

7. Study of the Reusability of the ZnO-NPs Photocatalyst:

The reusability and stability of photocatalysts are important aspects worthy of investigation. This study evaluated the reusability of the ZnO photocatalyst under sunlight and UV light using identical reaction conditions. The ZnO photocatalyst was separated by centrifugation at 3000 rpm for 10 minutes, then washed with ethanol and deionized water, dried, and reused for subsequent photocatalytic degradation cycles of MB dye.

The results presented in Figure 9 demonstrate four consecutive reuse cycles with promising outcomes. It is noteworthy that the photocatalyst efficiency may decline due to adsorption of degradation by-products on its surface, which can damage active sites and reduce catalytic performance. Additionally, loss of catalyst material during washing and drying may contribute to decreased efficiency. Nevertheless, the ZnO photocatalyst maintained a degradation efficiency of 86.7% even after the fourth cycle, indicating excellent reusability and stability.

Therefore, ZnO photocatalyst represents a suitable and promising candidate for the treatment of wastewater contaminated with organic dyes and pollutants.

DOI: https://doi.org/10.5281/zenodo.23287208

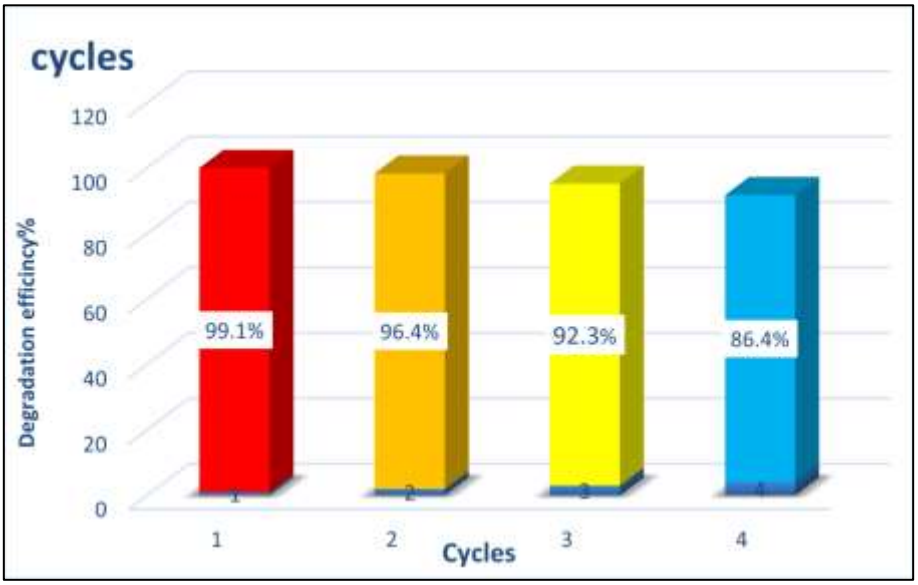


Fig. 9: Graphs illustrating the reusability test data of the ZnO photocatalyst for the degradation of MB dye under sunlight.

Conclusions

In this study, we successfully synthesized a novel, versatile ZnO nanoparticle photocatalyst via a green method using banana peel extract—an eco-friendly, simple, and cost-effective approach. The prepared ZnO nanoparticles were thoroughly characterized using various techniques including FT-IR, XRD, FE-SEM, AFM, EDX, and UV-Vis spectroscopy. The new ZnO photocatalyst demonstrated excellent performance, achieving a high degradation efficiency of 99.1% for methylene blue (MB) dye under UV light within 60 minutes, and 98.2% photodegradation efficiency under sunlight over 180 minutes. Optimal conditions to maximize photocatalytic efficiency were determined, including catalyst dosage (0.05 g/L), pH range (2–10), MB dye concentration (10 ppm), and identifying UV and sunlight as the most effective light sources. Importantly, the catalyst could be easily recovered from contaminated solutions, enhancing operational convenience and efficiency in water treatment. Furthermore, the study confirmed the remarkable stability of the ZnO nanocomposite, evidenced by its capability to be reused for four consecutive cycles with minimal loss in activity, underscoring its practical potential for sustainable environmental applications in the removal of organic pollutants and dyes from wastewater.

References

[1] Saratale RG, Saratale GD, Chang JS, Govindwar SP. Methylene blue dye: Toxicity, absorption and removal methods from wastewater. Environ Chem Lett. 2022. doi:10.1007/s10311-021-01284-0

[2] Ahmed MJ, Hameed BH. Photocatalytic degradation of methylene blue dye using metal oxide nanoparticles: A review. J Environ Manage. 2020. doi:10.1016/j.jenvman.2020.111019

[3] Weldekirstos HD, Mengist T, Belachew N, Mekonnen ML. Enhanced photocatalytic degradation of methylene blue dye using facilely synthesized g-C3N4/CoFe2O4 composite under sunlight irradiation. Results Chem. 2024;7:101306.

[4] Cai C, Han S, Liu W, Sun K, Qiao L, Li S, et al. Tuning catalytic performance by controlling reconstruction process in operando condition. Appl Catal B Environ. 2020;260:118103. doi:10.1016/j.apcatb.2019.118103

DOI: https://doi.org/10.5281/zenodo.23287208

[5] Katubi KM, Murtaza A, Asif HM, Alrowaili ZA, Al-Buriahi MS, Munir S, et al. Fabrication and characterization of ternary composite MgFe2O4/MoO3@CNTs for the enhanced photocatalytic activity to degrade organic pollutants. J Alloys Compd. 2024;978:173327. doi:10.1016/j.jallcom.2023.173327

[6] Othman I, Banat F, Hasan SW, Aubry C, Suresh S, Sillanpää M, et al. Facile preparation of magnetic CuFe2O4 on sepiolite/GO nanocomposites for efficient removal of Pb(II) and Cd(II) from aqueous solution. ACS Omega. 2023;8:38828–38838. doi:10.1021/acsomega.3c02006

[7] Chand M, Barthwal S, Rawat AS, Khanuja M, Rawat S. Enhancing photocatalytic efficiency of spent tea leaf powder on ZnIn2S4 incorporation: Role of surface charge on dye degradation. ACS Omega. 2023;8:17880–17890. doi:10.1021/acsomega.3c00955

[8] Ren F, Li Z, Tan WZ, Liu XH, Sun ZF, Ren PG, et al. Facile preparation of 3D regenerated cellulose/graphene oxide composite aerogel with high-efficiency adsorption towards methylene blue. J Colloid Interface Sci. 2018;532:58–67. doi:10.1016/j.jcis.2018.07.101

[9] Haounati R, El Guerdaoui A, Ouachtak H, El Haouti R, Bouddouch A, Hafid N, et al. Design of direct Z-scheme superb magnetic nanocomposite photocatalyst Fe3O4/Ag3PO4@Sep for hazardous dye degradation. Sep Purif Technol. 2021;277:119399. doi:10.1016/j.seppur.2021.119399

[10] Abdallah NIM, Li Y, Wang XT, Li X, Wang CW. Design and fabrication of Ni(OH)2/BiVO4 heterostructured nano-photocatalyst for high-efficient removal of organic dyes. J Alloys Compd. 2020;831:154828. doi:10.1016/j.jallcom.2020.154828

[11] Fahmi Abbas R, Hassan MMJ, Rheima AM. Adsorption of Fast Green dye onto Fe3O4 MNPs and GO/Fe3O4 MNPs synthesized by photo-irradiation method: Isotherms, thermodynamics, kinetics, and reuse studies. Sustain Chem Environ. 2024;6(1):100104.

[12] Kumar A, Sharma G, Naushad M, Ghfar AA, Alqadami AA, Bhatnagar A. Efficient removal of fast green dye from wastewater using eco-friendly magnetic chitosan nanocomposite: Modeling and mechanism. J Clean Prod. 2019;231:732–744.

[13] Othman Z, Sinopoli A, Mackey HR, Mahmoud KA. Efficient photocatalytic degradation of organic dyes by AgNPs/TiO2/Ti3C2Tx MXene composites under UV and solar light. ACS Omega. 2021;6:33325–33338. doi:10.1021/acsomega.1c03189

[14] Xu X, Lin X, Yang F, Huang S, Cheng X. Piezo-photocatalytic activity of Bi0.5Na0.5TiO3@TiO2 composite catalyst with heterojunction for degradation of organic dye molecule. J Phys Chem C. 2020;124:24126–24134. doi:10.1021/acs.jpcc.0c04700

[15] Mittal A, et al. Adsorptive removal of a dye using Indian basil powder. J Colloid Interface Sci. 2007;315(1):87–93.

[16] Karthik L, et al. Biosynthesis of Fe2O3 nanoparticles and their applications. Mater Lett. 2014;132:52–55.

[17] Kalaycıoğlu Z, Uysal BÖ, Pekcan Ö, Erim FB. Efficient photocatalytic degradation of methylene blue dye from aqueous solution with cerium oxide nanoparticles and graphene oxide-doped polyacrylamide. ACS Omega. 2023;8:13004–13015. doi:10.1021/acsomega.3c00198

[18] Borthakur S, Saikia L. ZnFe2O4@g-C3N4 nanocomposites: An efficient catalyst for Fenton-like photodegradation of rhodamine B. J Environ Chem Eng. 2019;7:103035. doi:10.1016/j.jece.2019.103035

[19] Sambaza S, Maity A, Pillay K. Enhanced degradation of BPA in water by PANI supported Ag/TiO2 nanocomposite under UV and visible light. J Environ Chem Eng. 2019;7:102880. doi:10.1016/j.jece.2019.102880

[20] Iravani S. Green synthesis of metal nanoparticles using plants. Green Chem. 2011;13(10):2638–2650.

DOI: https://doi.org/10.5281/zenodo.23287208

[21] Bhuyan A, Ahmaruzzaman M. Recent advances in MOF-5-based photocatalysts for efficient degradation of toxic organic dyes in aqueous medium. Next Sustain. 2024;3:100016. doi:10.1016/j.nxsust.2023.100016

[22] Samarasinghe LV, Muthukumaran S, Baskaran K. Recent advances in visible light-activated photocatalysts for degradation of dyes: A comprehensive review. Chemosphere. 2024;349:140818. doi:10.1016/j.chemosphere.2023.140818

[23] Nasrollahzadeh M, et al. Green synthesis of iron-based nanoparticles using plant extracts. Chem Eng J. 2021;408:127246.

[24] Mandal B, Panda J, Paul PK, Sarkar R, Tudu B. MnFe2O4 decorated reduced graphene oxide heterostructures: Nanophotocatalyst for methylene blue dye degradation. Vacuum. 2020;173.

[25] Elizabeth AT, James E, Jesan LI, Arockiaraj SD, Vasu AE. Green synthesis of value-added nitrogen doped carbon quantum dots from Crescentia cujete fruit waste for selective sensing of Fe3+ ions in aqueous medium. Inorg Chem Commun. 2023;149:110427.

[26] Liu Z, Li N, Liu P, Qin Z, Jiao T. Highly sensitive detection of iron ions in aqueous solutions using fluorescent chitosan nanoparticles functionalized by rhodamine B. ACS Omega. 2022;7(6):5570–5577.

[27] Aguiar JIS, Ribeiro SO, Leite A, Rangel M, Rangel AOSS, Mesquita RBR. Iron determination in natural waters using a synthesised 3-hydroxy-4-pyridione ligand in a newly developed microfluidic paper-based device. Chemosensors. 2023;11(2):101.

[28] Mishra S, Acharya R, Parida K. Spinel-ferrite-decorated graphene-based nanocomposites for enhanced photocatalytic detoxification of organic dyes in aqueous medium: A review. Water (Basel). 2023;15:81. doi:10.3390/w15010081

[29] Esharan K, Pillay K, Oluwafemi OS. Sunlight-driven photocatalytic degradation of methylene blue dye using a green synthesized ZnO–biochar composite from banana peels. Biomass Convers Biorefin. 2024. doi:10.1007/s13399-024-05999-z

[30] Pillay K, Esharan K, Oluwafemi OS. Antimicrobial and photocatalytic potential of a ZnO–biochar nanocomposite derived from banana peels for wastewater treatment. Water Air Soil Pollut. 2024;236(5):189. doi:10.1007/s11270-025-08189-3

[31] Ye J, Liu SQ, Liu WX, Meng ZD, Luo L, Chen F, et al. Photocatalytic simultaneous removal of nitrite and ammonia via a zinc ferrite/activated carbon hybrid catalyst under UV–visible irradiation. ACS Omega. 2019;4:6411–6420. doi:10.1021/acsomega.8b00677

[32] Krishnan K. X-ray diffraction. In: 2021. doi:10.1093/oso/9780198830252.003.0007

[33] Yu C, Wang CF, Chen S. Facile access to graphene oxide from ferro-induced oxidation. Sci Rep. 2016;6:17071. doi:10.1038/srep17071

[34] Doumeng M, Makhlouf L, Berthet F, Marsan O, Delbé K, Denape J, et al. A comparative study of the crystallinity of polyetheretherketone by using density, DSC, XRD, and Raman spectroscopy techniques. Polym Test. 2021;93:106878. doi:10.1016/j.polymertesting.2020.106878

[35] Boppudi HB, et al. Zinc oxide nanoparticles as an efficient antioxidant, photocatalyst, and heterogeneous catalyst in C–P bond synthesis. Results Chem. 2023;6:101227.

[36] Kadhim DA, Abid MA, Salih WM. Development of iron oxide nanoparticles using egg peel (brown) extract as a useful tool for removing the MB dye. Mater Sci Eng B. 2024;300:117104.

[37] Theivasanthi T, Alagar M. X-ray diffraction studies of copper nanopowder. 2010;1(2):112–117.

[38] Mohammadyani D. Characterization of nickel oxide nanoparticles synthesized via rapid microwave-assisted route. 2012;5:270–276.

DOI: https://doi.org/10.5281/zenodo.23287208

[39] Taglieri G, et al. New eco-friendly and low-energy synthesis to produce ZnO nanoparticles for real-world scale applications. Nanomaterials. 2023;13(17):2458.
[40] Sato M, Konomi M, Tamochi R, Ishikawa T. Development of FE-SEM technologies for life science fields. 2019. doi:10.1002/9781118663233.ch3.
[41] Handore K, et al. Novel green route of synthesis of ZnO nanoparticles by using natural biodegradable polymer and its application as a catalyst for oxidation of aldehydes. J Macromol Sci A. 2014;51(12):941–947.
[42] Sundaram RS, Venkataraj S, Muthuraman V. Synthesis and FTIR analysis of ZnO nanoparticles. Int J Sci Res Educ. 2015;3(6):3930–3935.
[43] Singh A, et al. Green synthesis of iron oxide nanoparticles using Ocimum basilicum and its application in photocatalysis. J Environ Chem Eng. 2022;10(3).
[44] Kumar P, et al. UV–Vis and Tauc analysis of green-synthesized ZnO nanoparticles. Mater Today Proc. 2023;56.
[45] Kareem BA, Alshabander BM. Influence of pH on the photocatalytic activity of Ag/ZnO and S/ZnO nanoparticles by methyl blue dye degradation. 2025.
[46] Naik B, Salker AV. Visible light driven photocatalytic degradation of textile dye over Fe2O3 nanoparticles. J Environ Chem Eng. 2018;6(1):363–373.
[47] Zhang X, Li Y, Wang J, Chen Z. Influence of catalyst loading on photocatalytic degradation performance of KBNNO. RSC Adv. 2020;10:12345–12352. doi:10.1039/D0RA01234A
[48] Lee S, Herrmann JM. Effect of catalyst agglomeration and light scattering on photocatalytic activity. J Photochem Photobiol A Chem. 2019;376:112–118. doi:10.1016/j.jphotochem.2019.01.015
[49] Eswaran P, Madasamy PD, Pillay K, Brink HG. Sunlight-driven photocatalytic degradation of methylene blue using ZnO/biochar nanocomposite derived from banana peels. Biomass Convers Biorefin. 2025;15:12347–12367.
[50] Islam KS, Mustak MH, Shishir MKH, Karim MM, Khan GMA. Biosynthesis of ZnO nanoparticles using banana peel pectin for antibacterial and photocatalytic applications. S Afr J Chem Eng. 2025;52:8–18.
[51] Meuseed KA, Mohammed AM, Al-Douri Y. Cellulose acetate-zinc oxide nanoparticle (CA-ZnO-NP) membranes for photocatalytic degradation of methylene blue dye: A comparative study under sunlight and UV irradiation. Environ Prog Sustain Energy. 2021;40(6):e14529. doi:10.1002/ep.14529
[52] Ali I, Basheer AA, Kumar S. Comparative study of photocatalytic fuel cell for degradation of methylene blue under sunlight and ultra-violet light irradiation. 2016.